Effect of anisotropy on the long-term strength of granite

Yoshitaka Nara*

Department of Civil and Earth Resources Engineering, Graduate School of Engineering, Kyoto University, Kyoto Daigaku Katsura, Nishikyo-ku, Kyoto 615-8540, Japan

Current Affiliation: Department of Management of Social Systems and Civil Engineering, Graduate School of Engineering, Tottori University, 4-101 Koyama-Minami, Tottori 680-8552, Japan

*Correspondence:

Department of Management of Social Systems and Civil Engineering, Graduate School of Engineering, Tottori University, 4-101 Koyama-Minami, Tottori 680-8552, Japan

E-mail: nara@kumst.kyoto-u.ac.jp

Tel & Fax: +81 857 31 5290

Abstract

Granite rock mass is used for various rock engineering purposes. To ensure long-term stability, information about the subcritical crack growth and an estimate of the long-term strength of the rock are necessary. The influence of the anisotropy of granite on its long-term strength has not yet been clarified. In this study, the anisotropy of the long-term rock strength was investigated for two types of granite rocks, Oshima granite and Inada granite. Specifically, the effect of the anisotropy in crack propagation on the long-term strength was examined. The results showed that the long-term strength of granite is anisotropic, as are the fracture toughness and Brazilian tensile strength measured in this study. The long-term strength was lowest when crack propagation occurred parallel to the rift plane, where most of the microcracks occur. For Inada granite, which has an anisotropic subcritical crack growth index, the degree of anisotropy of the long-term strength increased as the time-to-failure increased. This suggests that the long-term strength of granite is anisotropic.

Keywords: Anisotropy; granite; subcritical crack growth; fracture toughness; long-term strength

1. Introduction

Granite rock mass has been used for various rock engineering and geomechanical purposes such as underground disposal of radioactive waste, construction of caverns to store liquid natural gas or liquid petroleum gas, and extraction of geothermal energy from hot dry rock. Granite contains numerous microcracks, and the distribution of these microcracks has a strong effect on the transport of mineral resources and geothermal energy underground. Therefore, knowledge of microcrack distribution in granite is essential for the safe and efficient use of granite for various geomechanical and engineering purposes.

Granite has physical and mechanical anisotropies arising from the preferred orientation of the microcracks (Dale 1923; Simmons et al. 1975; Sano et al. 1992). Various researchers have reported the anisotropy of elastic wave velocities in granite. For example, Thill et al. (1973) reported that P-wave velocity had orthorhombic anisotropy in both saturated and dry rock conditions, and that this anisotropy is related to the preferred orientation of the microcracks. Sano et al. (1992) reported that granite generally had orthorhombic elasticity, as demonstrated by measuring P-wave and S-wave velocities in 18-faced and 34-faced polyhedral specimens of Barre granite, Chelmsford granite, and Oshima granite. They also concluded that the granite anisotropy was caused by the preferred orientation of the microcracks because the anisotropy disappeared when the microcracks were closed under hydrostatic pressure greater than 100 MPa. Takemura et al. (2003) and Takemura and Oda (2005) showed that the anisotropy of the P-wave velocity in Inada granite and Oshima granite was caused by the distribution of open microcracks. Nara et al. (2011) reported that P-wave velocities in granite

could be generally approximated by the associated Legendre function, which is extended to second-order terms by determining the three-dimensional distribution of P-wave velocity in polyhedral granite specimens.

Since granite rock mass is used for various rock engineering purposes as mentioned before, it is essential to study fracturing in granite to ensure the mechanical stability of granite rock mass. Rock strength measured in laboratory tests is anisotropic (Douglass and Voight 1969; Peng and Johnson 1972). In granite, the preferred orientation of microcracks affects fracture propagation. Nara et al. (2006) and Fujii et al. (2007) reported that the roughness of the crack path and fracture plane was reduced in fracturing that was parallel to the rift plane, where most microcracks occur. Their results indicate that fracturing in granite connects microcracks distributed parallel to the crack propagation direction. Sano and Kudo (1992) and Nara and Kaneko (2006) found that crack velocity in granite was anisotropic by measuring the subcritical crack growth (SCG) (Anderson and Grew 1977; Atkinson 1984). Specifically, Nara and Kaneko (2006) reported that the crack velocity was highest if the crack propagated parallel to the rift plane.

SCG is the main cause of time-dependent fracturing in rock. By measuring SCG, it is possible to estimate the long-term strength (LTS) of rock (Nara et al. 2010, 2013). LTS information is essential to ensure the long-term integrity of the rock mass. Since we have a good understanding of the anisotropy of granite, it is important to consider the anisotropy of granite in the estimation of LTS. However, the estimation of LTS was conducted by assuming that the materials were isotopic (Nara et al. 2010; 2013), and information about the

anisotropy of granite LTS is not widely available.

In this study, using granite samples, the anisotropy of LTS is investigated. Specifically, the effect of anisotropic crack propagation on LTS is examined by analyzing SCG in granite.

2. Rock samples

Oshima granite (OG) and Inada granite (IG) are used as the rock samples (Fig. 1). Figures 2 and 3 show photomicrographs of OG and IG where panels a, b, and c present photomicrographs obtained under ultraviolet light by the fluorescent method (Ali and Weiss 1968; Gardner and Pincus 1968; Nishiyama and Kusuda 1994), open nicol, and crossed nicols, respectively. The constituent minerals (proportion) of OG are quartz (36%), plagioclase (37%), K-feldspar (22%), biotite (4%), and hornblende (less than 1%) (Sano et al. 1981). IG consists of quartz (36%), plagioclase (32%), K-feldspar (28%), biotite (4%), and trace amounts of accessory minerals such as allanite, zircon, apatite, and ilmenite. (Lin 2002).

It has been reported that some granitic rocks have foliation (Kanaori et al. 1991). In this study, however, the effect of foliation on the property of granite is not discussed because the granite samples used in this study were obtained from the same quarry as the samples used by Sano and Kudo (1992) for OG and Lin (2002) for IG, which were found to have no foliation.

Orthorhombic elasticity was observed in OG and IG (Sano and Kudo 1992; Sano et al. 1992; Nara and Kaneko 2006). Especially, Nara and Kaneko (2006) measured P- and S-wave velocities in OG and IG granite samples similar to those used in this study and reported that the samples had orthorhombic elasticity due to the preferred orientation of pre-existing

microcracks. Nara and Kaneko (2006) named three principal axes (axes-1, -2, and -3) in descending order of P-wave velocity propagating parallel to these axes. The planes normal to axes-1, -2, and -3 are planes-1, -2, and -3, respectively. Therefore, plane-3 corresponds to the rift plane in granite. The values of P-wave velocity propagating normal to these planes in OG and IG are summarized in Table 1. In Tables 2 and 3, the orthorhombic elastic compliances of OG and IG, respectively, are summarized (Nara and Kaneko, 2006).

Sano and Kudo (1992) and Nara and Kaneko (2006) reported anisotropy in the relation between the stress intensity factor, K_I, and the crack velocity, da/dt (the K_I-da/dt relationship) for SCG in granite, verified by the double torsion (DT) test (Williams and Evans, 1973). In particular, Nara and Kaneko (2006) clarified that the opening direction of the crack controlled the K_I-da/dt relationship for granite. This means that the properties of tensile fracturing in granite are controlled by the preferred orientation of the pre-existing microcracks.

3. Methodology

3.1 Estimating the long-term strength

To estimate the LTS, we assume an infinite plate containing a single crack of length 2a, subjected to a uniform tensile stress σ (Murakami, 1986). In this case, the stress intensity factor is expressed by

$$K_I = \sigma(\pi a)^{1/2} \qquad (1)$$

where K_I is the mode-I stress intensity factor.

The relationship between the crack velocity and the stress intensity factor is expressed as follows (Charles, 1958):

$$\frac{\mathrm{d}a}{\mathrm{d}t} = AK_{\mathrm{I}}^{\,n} \qquad (2)$$

where da/dt is the crack velocity, and A and n are experimentally determined constants, called SCG parameters (Nara et al. 2013); in particular, n is the SCG index (Atkinson 1984; Atkinson and Meredith 1987). From Eqs. (1) and (2), the following equation can be obtained:

$$\frac{\mathrm{d}a}{\mathrm{d}t} = \pi^{n/2} A\sigma^n a^{n/2} \qquad (3)$$

From this equation we obtain

$$\int a^{-n/2}\mathrm{d}a = \int \pi^{n/2} A\sigma^n \mathrm{d}t \qquad (4)$$

The general solution of Eq. (4) is

$$\frac{1}{1\text{-}n/2} a^{1-n/2} = \pi^{n/2} A\sigma^n t + c \qquad (5)$$

where c is a constant of integration. For initial condition $a = a_0$ at $t = 0$, the constant c is given by

$$\frac{2}{2\text{-}n} a_0^{(2-n)/2} = c \qquad (6)$$

From Eqs. (5) and (6), the following equation can be obtained:

$$a^{(2-n)/2} = \frac{2-n}{2}\pi^{n/2} A\sigma^n t + a_0^{(2-n)/2} \qquad (7)$$

Then, from Eq. (7) we obtain

$$t = \frac{2}{(n-2)\pi^{n/2} A}\frac{a_0^{(2-n)/2}}{\sigma^n}\left\{1-\left(\frac{a}{a_0}\right)^{(2-n)/2}\right\} \qquad (8)$$

Even though the crack propagates statically at the beginning, the manner of crack propagation will change from static to dynamic as time goes by. Furthermore, the crack length will increase rapidly and then diverge. Assuming that the time when the crack length diverges is the "time-to-failure" t_{f}, this is expressed as

$$t_f = \frac{2}{(n-2)\pi^{n/2}A}\frac{a_0^{(2-n)/2}}{\sigma^n} \quad (9)$$

For a material that reaches failure in x years under constant stress, the constant stress corresponds to the LTS. Because the time-to-failure is x years (about $3.15 \times 10^7 x$ seconds) under this stress, from Eq. (9) the following equation can be obtained:

$$(S_t(x))^n = \frac{1}{3.15\times10^7 x}\frac{2}{(n-2)\pi^{n/2}A}a_0^{(2-n)/2} \quad (10)$$

where $S_t(x)$ is the LTS.

If the tensile strength and the fracture toughness of a material are S_t and K_{IC}, respectively, then when the crack length is a_0, the relation between S_t and K_{IC} can be expressed as

$$K_{IC} = S_t(\pi a_0)^{1/2} \quad (11)$$

From Eqs. (10) and (11), we can then obtain the following equation:

$$S_t(x) = \left\{\frac{1}{3.15\times10^7 x}\frac{2}{(n-2)\pi A}\right\}^{1/n}\left(\frac{K_{IC}}{S_t}\right)^{(2-n)/n} \quad (12)$$

By using this equation, we can estimate the LTS of a solid material as $S_t(x)$ (Nara et al. 2010).

3.2 Estimation method of tensile strength and fracture toughness

In this study, the Brazilian tensile strength (splitting tensile strength) is used for S_t. To estimate the LTS of granite, the values of n, A, S_t, and K_{IC} are necessary.

The values for the SCG parameters n and A are taken from the results of Nara and Kaneko (2006); these were obtained in air in controlled temperature (284 K) and relative humidity (45%).

S_t and K_{IC} are experimentally measured in this study in ambient air conditions, without controlling temperature and relative humidity, because the loading frame used for the strength

measurements was not in a controlled environment. The temperature and relative humidity during the measurement of S_t and K_{IC} were 289–293 K and 45–50%, respectively.

S_t is measured by the Brazil test technique for a strain rate of 10^{-5} s^{-1} by preparing cylindrical specimens from the same blocks of OG and IG used in Nara and Kaneko (2006). The diameter and length of the specimens used in the Brazil test are 30 mm and 20 mm, respectively. The specimens were prepared from three orthogonal directions parallel to planes-1, -2, and -3 to investigate the strength anisotropy. The Brazilian tensile strength can be calculated from the following equation (Fairbairn and Ulm 2002):

$$S_t = \frac{2P_t}{\pi D l} \qquad (13)$$

where P_t is the applied load at failure, D is the diameter of the specimen, and l is the length of the specimen for the Brazil test.

The fracture toughness K_{IC} can be measured by the constant displacement rate method of the DT test (Evans 1972; Shyam and Lara-Curzio 2006). Figure 4 shows a schematic of the specimen for the DT testing. In this figure, the specimen dimensions are W – width, d – thickness, d_n – reduced thickness, and L – length. According to the reports of Evans et al. (1974), Atkinson (1979), and Pletka et al. (1979), the size of the DT specimen has to satisfy the following condition:

$$12d \le W \le L/2 \qquad (14)$$

Based on this condition, the size of the DT specimens in this study was set to W = 45 mm, d = 3 mm, d_n = 2 mm. The length L was set as 155 mm for OG while the length of the IG specimen was 110 mm, because the size of the IG block was smaller. The specimen sizes in

this study satisfy the condition of Eq. (14).

In Fig. 5, a photo and illustration of the experimental apparatus for the constant displacement rate method of DT testing are shown (Nara et al. 2012). This apparatus consists of a speed-control motor that drives the loading axis. The applied load is measured by a load cell with an accuracy of ±0.04 N. The displacement of the load-points is measured by two displacement transducers, each with an accuracy of ±0.5 μm.

The displacement rate should be higher than 0.07 mm/s, according to Selçuk and Atkinson (2000). In this study, following the method of Nara et al. (2012), K_{IC} is measured by using the constant displacement rate method of DT testing, applying a load at a displacement rate of 0.23 mm/s, the maximum rate of the experimental apparatus, and after applying a small amount of pre-load, around 10 N.

Figure 6 shows the temporal changes of the applied load on the DT specimens for the K_{IC} measurements. The time interval of the data sampling for the fracture toughness measurement was 0.5 s. The change of the applied load is very rapid. Using the peak value of the applied load, K_{IC} is estimated from the equations shown in Nara et al. (2012). For orthorhombic materials, assuming that the directions of the coordinate axes and loading are defined as given in Fig. 4, the fracture toughness K_{IC} can be expressed as follows:

$$K_{IC} = \left(\frac{3{P_{max}}^2 w_m s_{66}}{2d^3 d_n (2s_{22}((s_{11}s_{22})^{1/2} + s_{12} + s_{66}/2))^{1/2}} \right)^{1/2} \qquad (15)$$

where P_{max} is the maximum value of the applied load, w_m is the moment arm (18 mm was used here), and s_{ij} (i, j = 1, 2, or 6) is the elastic compliance of the orthorhombic material

(Sano and Kudo 1992; Nara and Kaneko 2006). As explained by Sano and Kudo (1992), if the loading direction is different from that given in Fig. 4, the subscripts of s_{ij} must be transformed.

4. Results

Photos of the DT specimens after the fracture toughness measurements are shown in Fig. 7. The specimens show complete failure due to the crack growth. In Table 4, the values of n, log$A$, S_t, and K_{IC} are summarized. All the values are with respect to the fracturing directions. The values of n were taken from Nara and Kaneko (2006), as mentioned before. Since the values of log A were not shown in Nara and Kaneko (2006), they were taken from the experimental results in Nara and Kaneko (2006) for this study. The value of K_{IC} for OG fracturing parallel to plane-3 was determined by using the relation between K_{IC} and the relative humidity that was experimentally obtained by Nara et al. (2012) and is expressed as follows:

$$K_{IC} = -2.41\times10^{-3} h_r + 2.27 \qquad (16)$$

where h_r is the relative humidity [%]. This was set as 50% for this study. In Table 4, the degree of anisotropy is also provided. The degree of anisotropy is calculated as (Max − Min)/Max, where Max and Min are the maximum and minimum values, respectively, of the parameter of interest. From Table 4, it can be seen that log$A$, S_t, and K_{IC} are anisotropic in all the cases. In addition, n is anisotropic for IG and isotropic for OG.

In Fig. 8, the relation between the LTS and time-to-failure for granite is shown. It can be seen that LTS is anisotropic for both types of granite rocks and is lowest when fracturing

occurs parallel to plane-3 (the rift plane). In Table 5, the values of LTS are summarized along with the degree of anisotropy, as in Table 4. The degree of LTS anisotropy for IG increases as the time-to-failure increases. In contrast, the degree of LTS anisotropy for OG is almost constant as the time-to-failure increases.

5. Discussion

This study found that LTS in granite is anisotropic. The experiments in this study also show that the tensile strength and fracture toughness are also anisotropic. Nara et al. (2010) described how to estimate LTS, and Nara et al. (2012) reported how to estimate the fracture toughness of rock using the DT test. However, their studies did not obtain the anisotropic properties of LTS and fracturing.

In this study, it was found that the Brazilian tensile strength and the fracture toughness were anisotropic. When fracturing occurred parallel to plane-3, the strength and fracture toughness were the smallest. This indicates that the preferred orientation of the pre-existing microcracks significantly affected the anisotropy of the strength and fracture toughness. Especially, the results suggest that the pre-existing microcracks parallel to the fracturing direction had a significant effect on the decrease of the strength and fracture toughness of the samples.

The granite samples OG and IG used in this study have physical and mechanical anisotropy. Using measurements of P- and S-wave velocities in various directions for OG and IG, Sano et al. (1992) and Nara and Kaneko (2006) reported that the anisotropy of granite in air and under low pressure was due to the preferred orientation of pre-existing microcracks. Using

various granite rocks quarried in Japan, Chen et al. (1999) and Nara et al. (2011) reported that the anisotropy of granite can be described by the distribution of the pre-existing microcracks. This suggests that granite in Japan generally has anisotropy due to the preferred orientation of pre-existing microcracks.

The anisotropy of LTS is caused by the strength and fracture toughness as well as the K_I-da/dt relationship for SCG. Therefore, determination of the SCG parameters n and A is important in understanding the characteristics of LTS. For the SCG parameters, A is anisotropic for both OG and IG, while n is anisotropic only for IG. The decrease in LTS with increasing time-to-failure is controlled by the value of n, because the slope in Fig. 5 is equal to $-1/n$, which comes from Eq. (12). When the value of n is higher, the decrease in LTS from increasing time-to-failure is smaller; therefore, the increased LTS anisotropy for IG is caused by the anisotropy of n.

The value of A corresponds to the crack velocity at $K_I = 1.0$ [MN/m$^{3/2}$] according to Eq. (2), and is directly related to the value of LTS at time-to-failure $t_f = 1$ [year] according to Eq. (12). Therefore, the value of A affects only the degree of LTS anisotropy at $t_f = 1$, $S_t(1)$.

For OG, even though n is isotropic, LTS is anisotropic. Since A is anisotropic for OG, it is considered that the estimate of A strongly affects the anisotropy of LTS. Ko and Kemeny (2013) reported that the value of A can be determined by various testing methods, including the DT test, Brazil test, three-point bending test, grooved disk test, and compact tension test. Additionally, they suggested that the deviation of A is largest for the DT test even though similar average values can be obtained. However, the DT test has the advantage that it can

provide the data of the crack velocity and the stress intensity factor which relate directly to the crack propagation. In addition, Nara and Kaneko (2006) already showed the dependence of the crack velocity in granite on the crack propagation direction. The value of A corresponds to the crack velocity at K_I = 1.0 MN/m$^{3/2}$. Therefore, the anisotropy of LTS shown in this study is considered to be valid. Furthermore, since n is significantly dependent on the crack propagation direction, the increase in the degree of LTS anisotropy for IG is also considered valid. The procedures in this study are therefore considered appropriate and the results are meaningful.

Because some rock engineering projects may be intended for long-term use, such as radioactive waste disposal, it is necessary to understand the time-dependent behavior of rocks, such as the SCG parameters (n and A) and the LTS. This study shows that the rock's LTS anisotropy can increase if n is anisotropic, and the LTS is lowest when the cracks propagate parallel to the weakest direction. Thus, the rock's suitability for use in an engineering project depends on whether it is anisotropic and on the lowest acceptable LTS value.

6. Conclusions

In this study, the anisotropy of granite LTS was investigated for two granite rocks (OG and IG). The influence of the anisotropy of crack propagation on granite-rock LTS was investigated. We found that the LTS of granite is anisotropic, as are the K_I-da/dt relation for SCG, the fracture toughness, and the Brazilian tensile strength. For both types of granite rock tested, the LTS was the lowest when crack growth occurred parallel to plane-3 (the rift plane). For IG, where both SCG parameters n and A are anisotropic, the degree of LTS anisotropy

increased with increasing time-to-failure. For OG, where *A* is anisotropic and *n* is isotropic, the degree of LTS anisotropy was independent of the time-to-failure even though the LTS was anisotropic. These results indicate that LTS is anisotropic for granite.

References

Ali SA, Weiss MP (1968) Fluorescent dye penetrant technique for displaying obscure structures in limestone. J Sediment Petrol 38:681-682

Anderson OL, Grew PC (1977) Stress corrosion theory of crack propagation with applications to geophysics. Rev Geophys Space Phys 15:77-104

Atkinson BK (1979) Fracture toughness of Tennessee sandstone and Carrara marble using the double torsion testing method. Int J Rock Mech Min Sci & Geomech Abstr 16:46-53

Atkinson BK (1984) Subcritical crack growth in geological materials. J Geophys Res 89:4077-4114

Atkinson BK, Meredith PG (1987) The theory of subcritical crack growth with applications to minerals and rocks. In: Atkinson BK (ed) Fracture Mechanics of Rock. Academic Press, London, pp 111-166

Charles RJ (1958) Static fatigue of glass II. J Appl Phys 29:1554-1560

Chen Y, Nishiyama T, Kusuda H, Kita H, Sato T (1999) Correlation between microcrack distribution patterns and granitic rock splitting planes. Int J Rock Mech Min Sci 36:535-541

Dale TN (1923) The commercial granites of New England, I. US Geol Surv Bull 738:22-103

Douglass PM, Voight B (1969) Anisotropy of granites: a reflection of microscopic fabric. Géotechnique 19:376-398

Evans AG (1972) A method for evaluating the time-dependent failure characteristics of brittle materials - and its application to polycrystalline alumina. J Mater Sci 7:1137-1146

Evans AG, Linzer M, Russell LR (1974) Acoustic emission and crack propagation in polycrystalline alumina. Mater Sci Eng 15:253-261

Fairbairn EMR, Ulm FJ (2002) A tribute to Fernando L. L. B. Carneiro (1913–2001) engineer and scientist who invented the Brazilian test. Mater Struct 35:195-196

Fujii Y, Takemura T, Takahashi M, Lin W (2007) Surface features of uniaxial tensile fractures

and their relation to rock anisotropy in Inada granite. Int J Rock Mech Min Sci 44:98-107

Gardner RD, Pincus HJ (1968) Fluorescent dye penetrants applied to rock fractures. Int J Rock Mech Min Sci 5:155-158

Kanaori Y, Kawakami S, Yairi K (1991) Microstructure of deformed biotite defining foliation in cataclasite zones in granite, central Japan. J Struct Geol 13:777-785

Ko TY, Kemeny J (2013) Determination of the subcritical crack growth parameters in rocks using the constant stress-rate test. Int J Rock Mech Min Sci 59:166-178

Lin W (2002) Permanent strain of thermal expansion and thermally induced microcracking in Inada granite. J Geophys Res. doi: 10.1029/2001JB000648

Murakami Y (1986) Stress Intensity Factors Handbook, Pergamon, Oxford

Nara Y, Kaneko K (2006) Sub-critical crack growth in anisotropic rock. Int J Rock Mech Min Sci 43:437-453

Nara Y, Koike K, Yoneda T, Kaneko K (2006) Relation between subcritical crack growth behavior and crack paths in granite. Int J Rock Mech Min Sci 43:1256-1261

Nara Y, Takada M, Mori D, Owada H, Yoneda T, Kaneko K (2010) Subcritical crack growth and long-term strength in rock and cementitious material. Int J Fract 164:57-71.

Nara Y, Kato H, Yoneda T, Kaneko K (2011) Determination of three-dimensional microcrack distribution and principal axes for granite using a polyhedral specimen. Int J Rock Mech Min Sci 48:316-335

Nara Y, Morimoto K, Hiroyoshi N, Yoneda T, Kaneko K, Benson PM (2012) Influence of relative humidity on fracture toughness of rock: Implications for subcritical crack growth. Int J Solids Struct 49:2471-2481

Nara Y, Yamanaka H, Oe Y, Kaneko K, (2013) Influence of temperature and water on subcritical crack growth parameters and long-term strength for igneous rocks. Geophys J Int 193:47-60

Nishiyama T, Kusuda H, (1994) Identification of pore spaces and microcracks using fluorescent resins. Int J Rock Mech Min Sci & Geomech Abstr 31:369-375

Peng S, Johnson AM (1972) Crack growth and faulting in cylindrical specimens of Chelmsford granite. Int J Rock Mech Min Sci 9:37-86

Pletka BJ, Fuller Jr ER, Koepke BG (1979) An evaluation of double-torsion testing – Experimental. ASTM STP 678, pp.19-37

Sano O, Kudo Y (1992) Relation of fracture resistance to fabric for granitic rocks. Pure Appl Geophys 138:657-677

Sano O, Ito I, Terada M (1981) Influence of strain rate on dilatancy and strength of Oshima granite under uniaxial compression. J Geophys Res 86:9299-9311

Sano O, Kudo Y, Mizuta Y (1992) Experimental determination of elastic constants of Oshima granite, Barre granite, and Chelmsford granite. J Geophys Res 97:3367-3379

Selçuk A, Atkinson A (2000) Strength and toughness of tape-cast yttria-stabilized zirconia. J Am Ceram Soc 83:2029-2035

Shyam A, Lara-Curzio E (2006) The double-torsion testing technique for determination of fracture toughness and slow crack growth behaviour of materials: a review. J Mater Sci 41:4093-4104

Simmons G, Todd T, Baldridge WS (1975) Toward a quantitative relationship between elastic properties and cracks in low porosity rocks. Am J Sci 275:318-345

Takemura T, Golshani A, Oda M, Suzuki K (2003) Preferred orientations of open microcracks in granite and their relation with anisotropic elasticity. Int J Rock Mech Min Sci 40:443-454

Takemura T, Oda M (2005) Changes in crack density and wave velocity in association with crack growth in triaxial tests of Inada granite. J Geophys Res. doi: 10.1029/2004JB003395

Thill RE, Bur TR, Steckley RC (1973) Velocity anisotropy in dry and saturated rock spheres and its relation to rock fabric. Int J Rock Mech Min Sci & Geomech Abstr 10:535-557

Williams DP, Evans AG (1973) A simple method for studying slow crack growth. J Test Eval 1:264-270

Figure captions

Figure 1 Photos of (a) Oshima granite and (b) Inada granite. The length and height are both 30 mm.

Figure 2 Photomicrographs of Oshima granite observed by a polarizing microscope under (a) ultraviolet light, (b) open nicol, and (c) crossed nicols. The height of each viewed area is 1.85 mm.

Figure 3 Photomicrographs of Inada granite observed by a polarizing microscope under (a) ultraviolet light, (b) open nicol, and (c) crossed nicols. The height of each viewed area is 1.85 mm.

Figure 4 Schematic of Double Torsion specimen and loading configuration. The loading forces are indicated by the four thick arrows.

Figure 5 Experimental apparatus for fracture toughness measurement. (a) Photo, (b) schematic illustration (after Nara et al. (2012)).

Figure 6 Temporal changes in applied load for fracture toughness measurements by constant displacement rate experiments of double torsion test. (a) Oshima granite

fracturing parallel to plane-1; (b) Oshima granite fracturing parallel to plane-2; (c) Inada granite fracturing parallel to plane-1; (d) Inada granite fracturing parallel to plane-2; (e) Inada granite fracturing parallel to plane-3.

Figure 7 Photos of Double Torsion specimen after fracture toughness measurements for (a) Oshima granite and (b) Inada granite. The length of the specimens for OG and IG are 155 mm and 110 mm, respectively.

Figure 8 Relation between long-term strength and time-to-failure for (a) Oshima and (b) Inada granite in air.

Table captions

Table 1 P-wave velocity in Oshima granite and Inada granite

Table 2 Elastic compliance of Oshima granite (after Nara and Kaneko (2006))

Table 3 Elastic compliance of Inada granite (after Nara and Kaneko (2006))

Table 4 Summary of subcritical crack growth parameters, fracture toughness, and tensile strength for granite

Table 5 Summary of long-term strength for granite

Table 1 P-wave velocity in Oshima granite and Inada granite

Rock samples	P-wave velocities [km/s]
Oshima granite	4.91 (in axis-1), 4.61 (in axis-2), 4.51 (in axis-3)
Inada granite	4.69 (in axis-1), 4.33 (in axis-2), 4.06 (in axis-3)

Table 2 Elastic compliance of Oshima granite (after Nara and Kaneko (2006)).

Elastic compliance s_{ij} [$\times 10^{-12}$Pa^{-1}]							
		j					
		1	2	3	4	5	6
i	1	16.7	−3.28	−3.28	0	0	0
	2	−3.28	18.9	−3.28	0	0	0
	3	−3.28	−3.28	19.7	0	0	0
	4	0	0	0	46.0	0	0
	5	0	0	0	0	43.4	0
	6	0	0	0	0	0	42.4

Table 3 Elastic compliance of Inada granite (after Nara and Kaneko (2006))

Elastic compliance s_{ij} [$\times 10^{-12}$Pa^{-1}]							
		j					
		1	2	3	4	5	6
i	1	18.1	−3.32	−3.32	0	0	0
	2	−3.32	21.1	−3.32	0	0	0
	3	−3.32	−3.28	23.9	0	0	0
	4	0	0	0	52.9	0	0
	5	0	0	0	0	49.1	0
	6	0	0	0	0	0	46.1

Table 4 Summary of subcritical crack growth parameters, fracture toughness, and tensile strength for granite

Rock samples	Fracturing direction	logA	n	Fracture toughness [MN/m$^{3/2}$]	Brazilian tensile strength [MPa]
Oshima granite	parallel to plane-1	−27.8±3.5	77±17	2.58±0.11	7.85±0.53
	parallel to plane-2	−25.6±2.4	79±10	2.27±0.06	6.39±0.13
	parallel to plane-3	−23.9±4.6	79±11	2.15 (after Nara et al. (2012))	6.14±0.06
	(Max − Min)/Max	0.140	0.026	0.167	0.218
Inada granite	parallel to plane-1	−19.3±3.3	75±11	1.89±0.09	10.04±0.39
	parallel to plane-2	−14.3±3.3	69±15	1.68±0.01	9.85±0.47
	parallel to plane-3	−9.9±2.8	54±12	1.30±0.09	6.58±0.21
	(Max − Min)/Max	0.487	0.280	0.312	0.345

Table 5 Summary of long-term strength for granite

Rock samples	Fracturing direction	$S_t(1)$ [MPa]	$S_t(10)$ [MPa]	$S_t(100)$ [MPa]	$S_t(1000)$ [MPa]	$S_t(10000)$ [MPa]
Oshima granite	parallel to plane-1	5.10	4.95	4.80	4.66	4.52
	parallel to plane-2	4.37	4.25	4.13	4.01	3.89
	parallel to plane-3	4.22	4.10	3.98	3.87	3.75
	(Max − Min)/Max	0.173	0.172	0.171	0.170	0.170
Inada granite	parallel to plane-1	6.85	6.64	6.44	6.25	6.06
	parallel to plane-2	6.57	6.36	6.15	5.95	5.75
	parallel to plane-3	4.87	4.66	4.47	4.28	4.10
	(Max − Min)/Max	0.289	0.298	0.306	0.315	0.323

Figure1a
Click here to download high resolution image

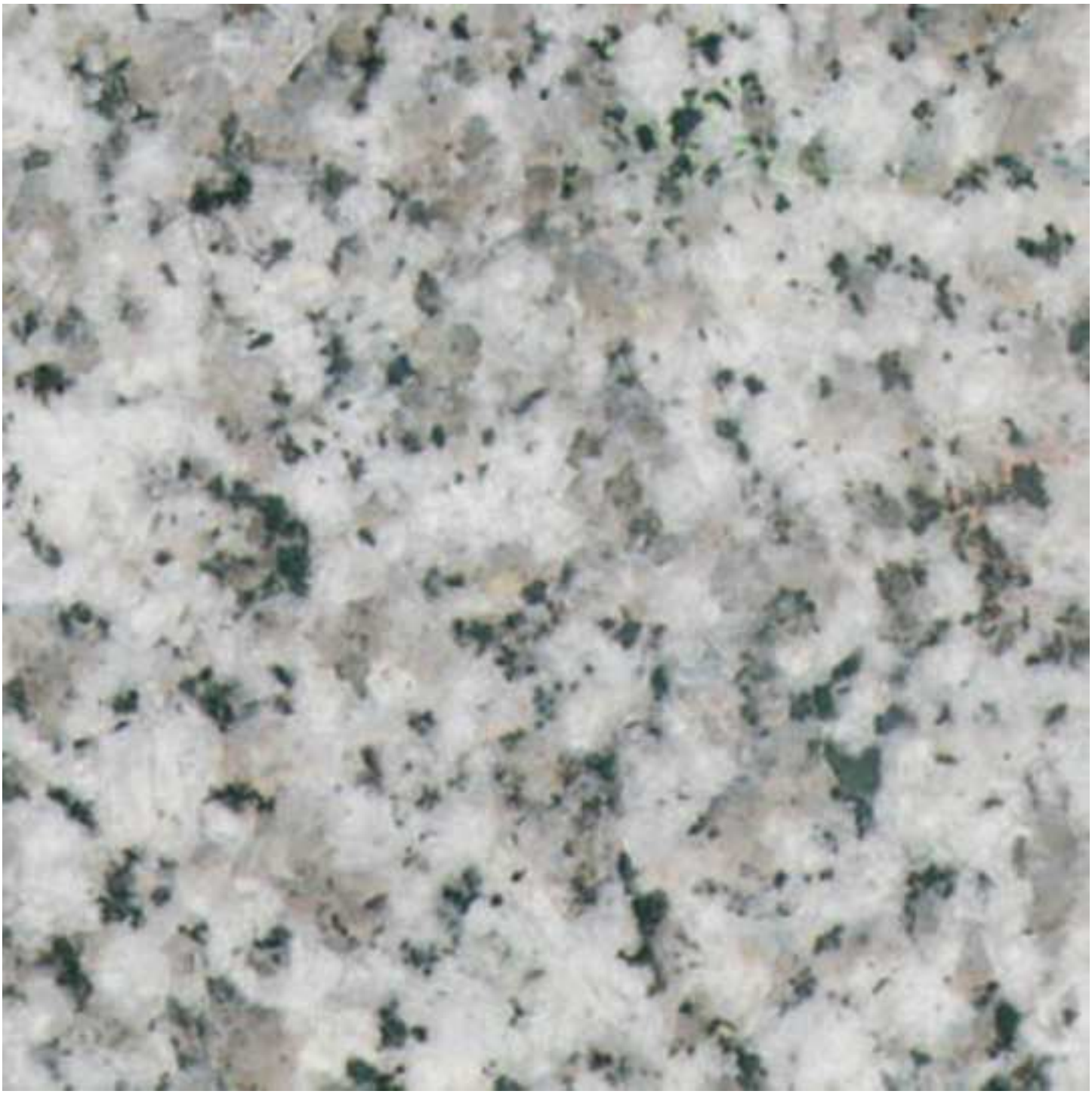

Figure1b
Click here to download high resolution image

Figure2a
Click here to download high resolution image

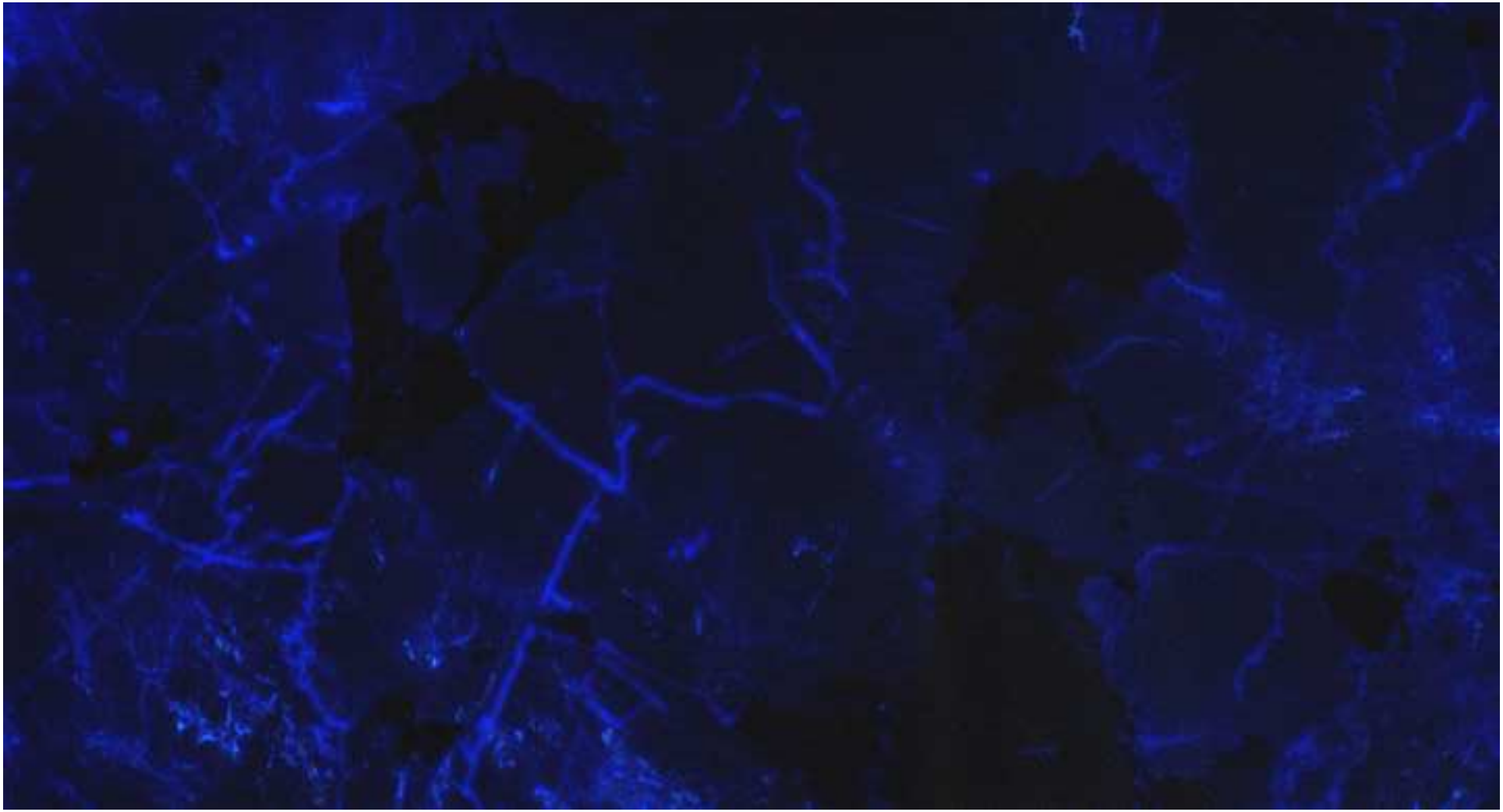

Figure2b
Click here to download high resolution image

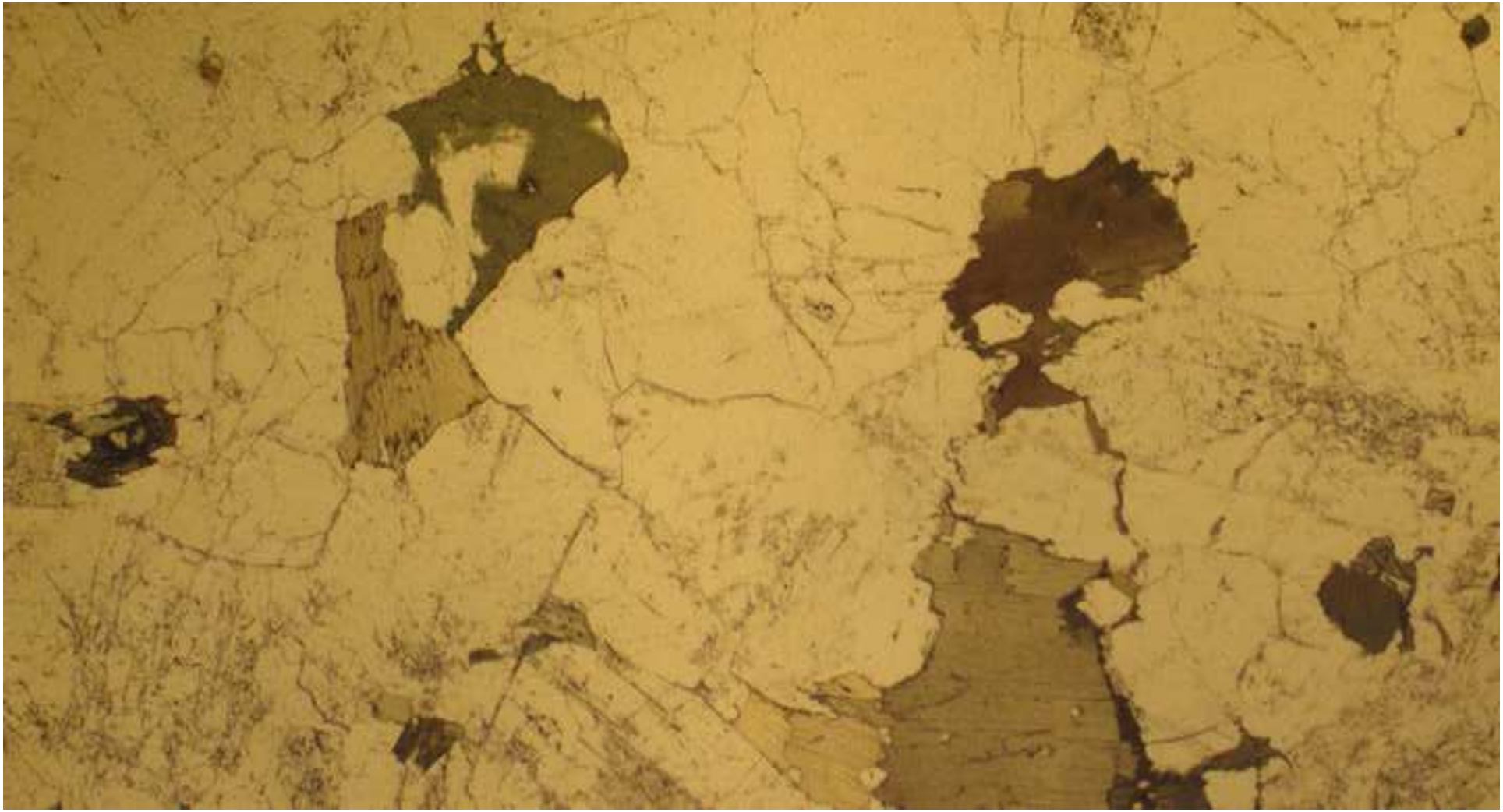

Figure2c
Click here to download high resolution image

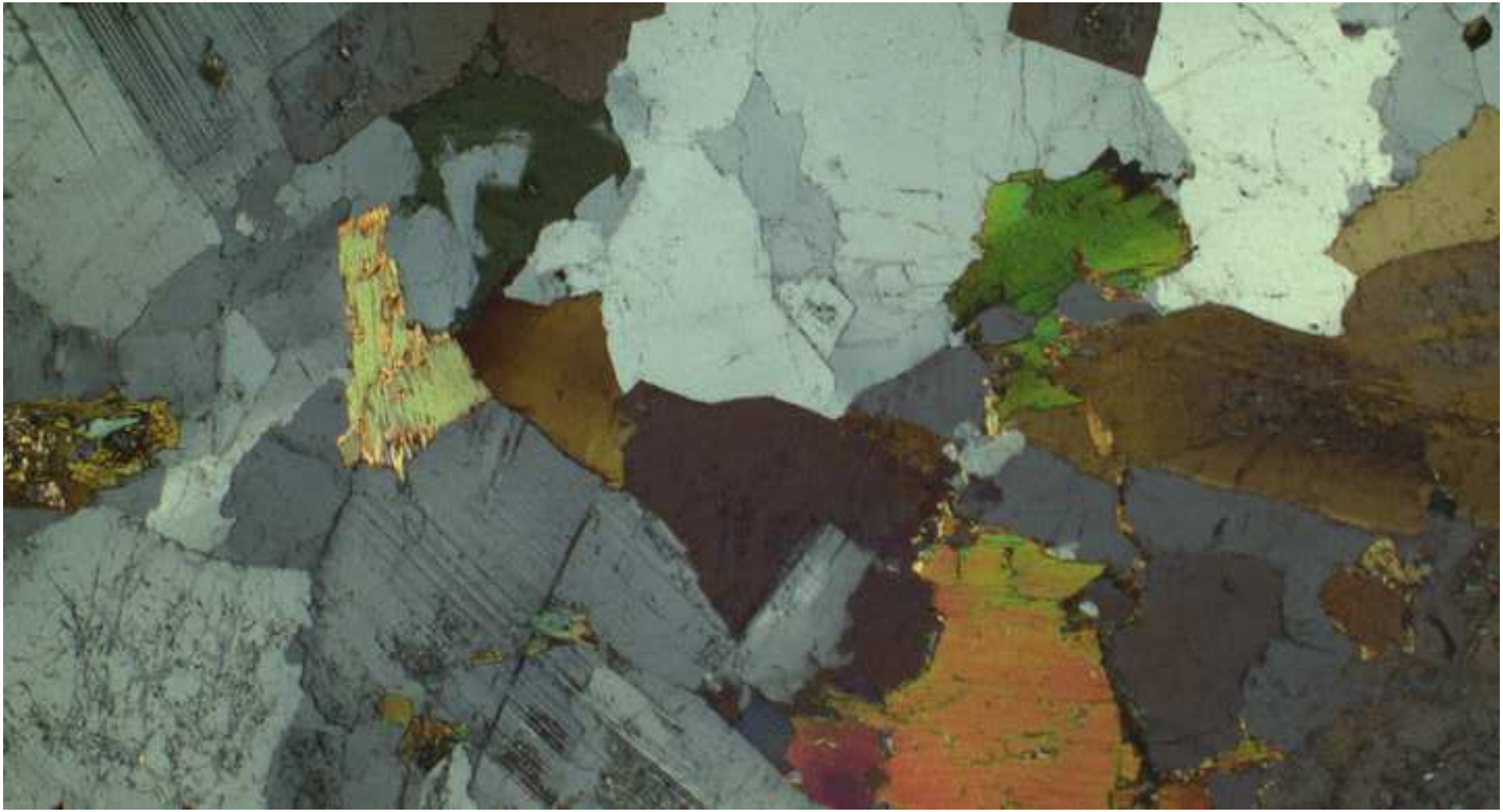

Figure3a
Click here to download high resolution image

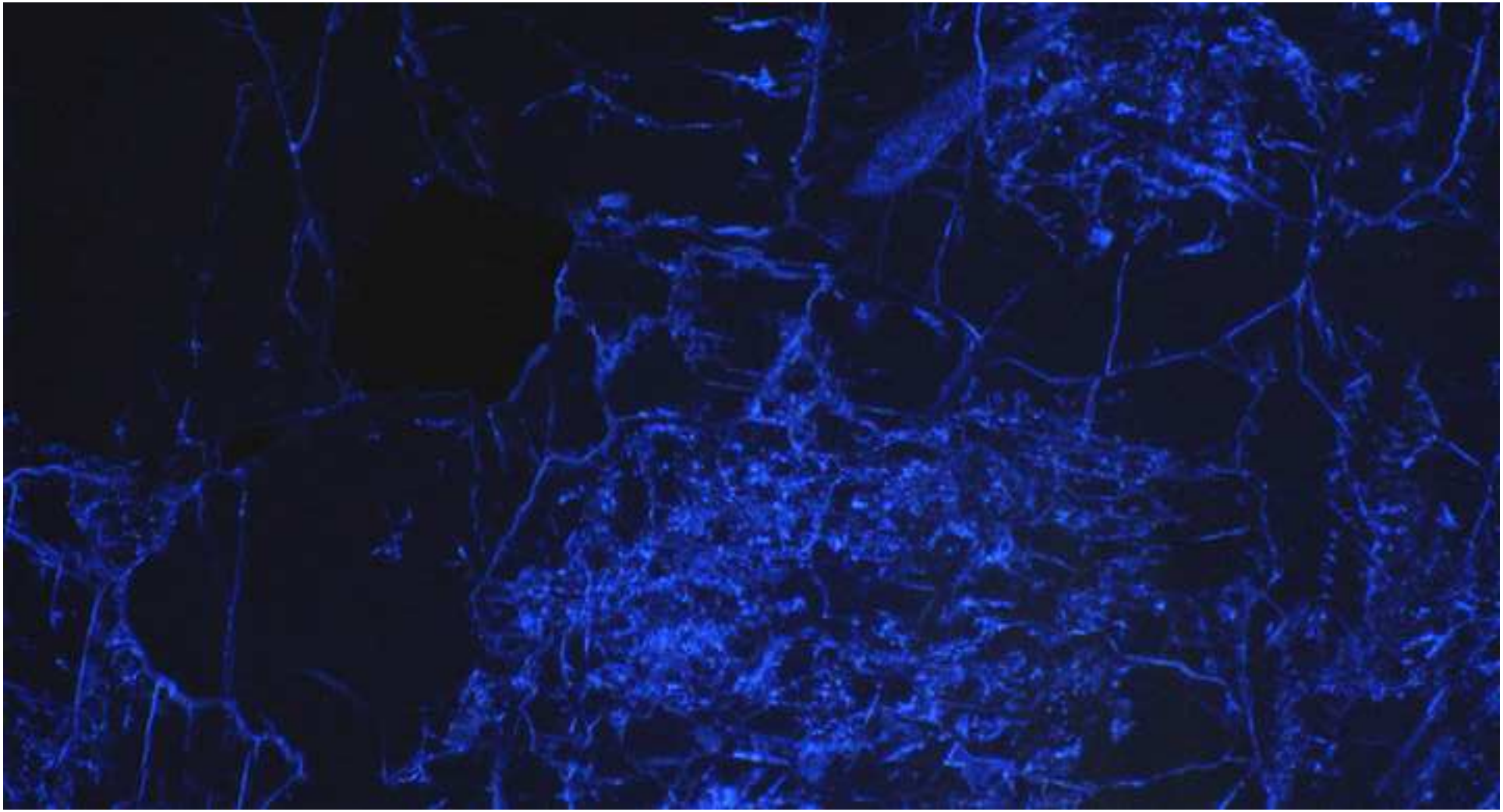

Figure3b
Click here to download high resolution image

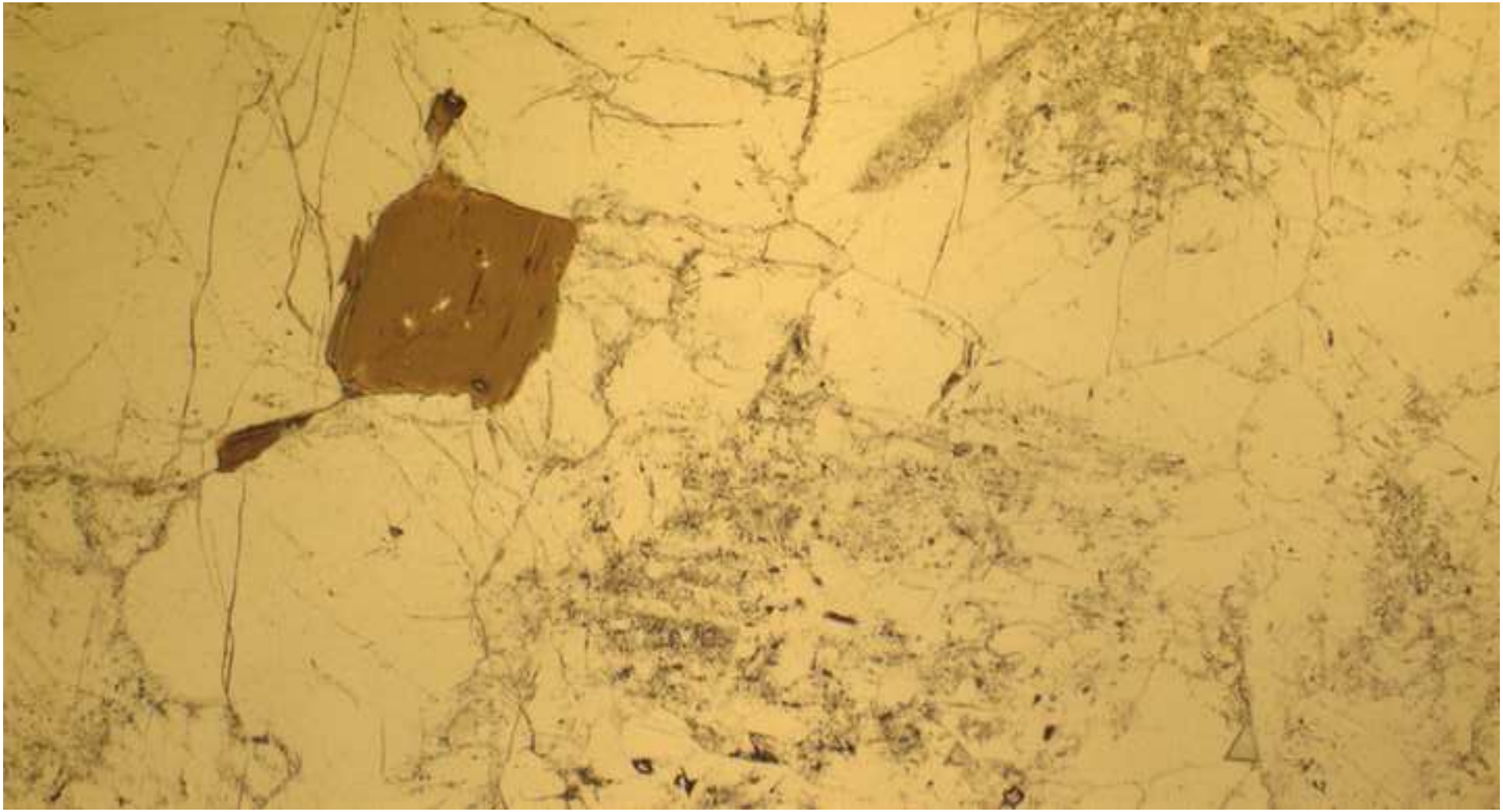

Figure3c
Click here to download high resolution image

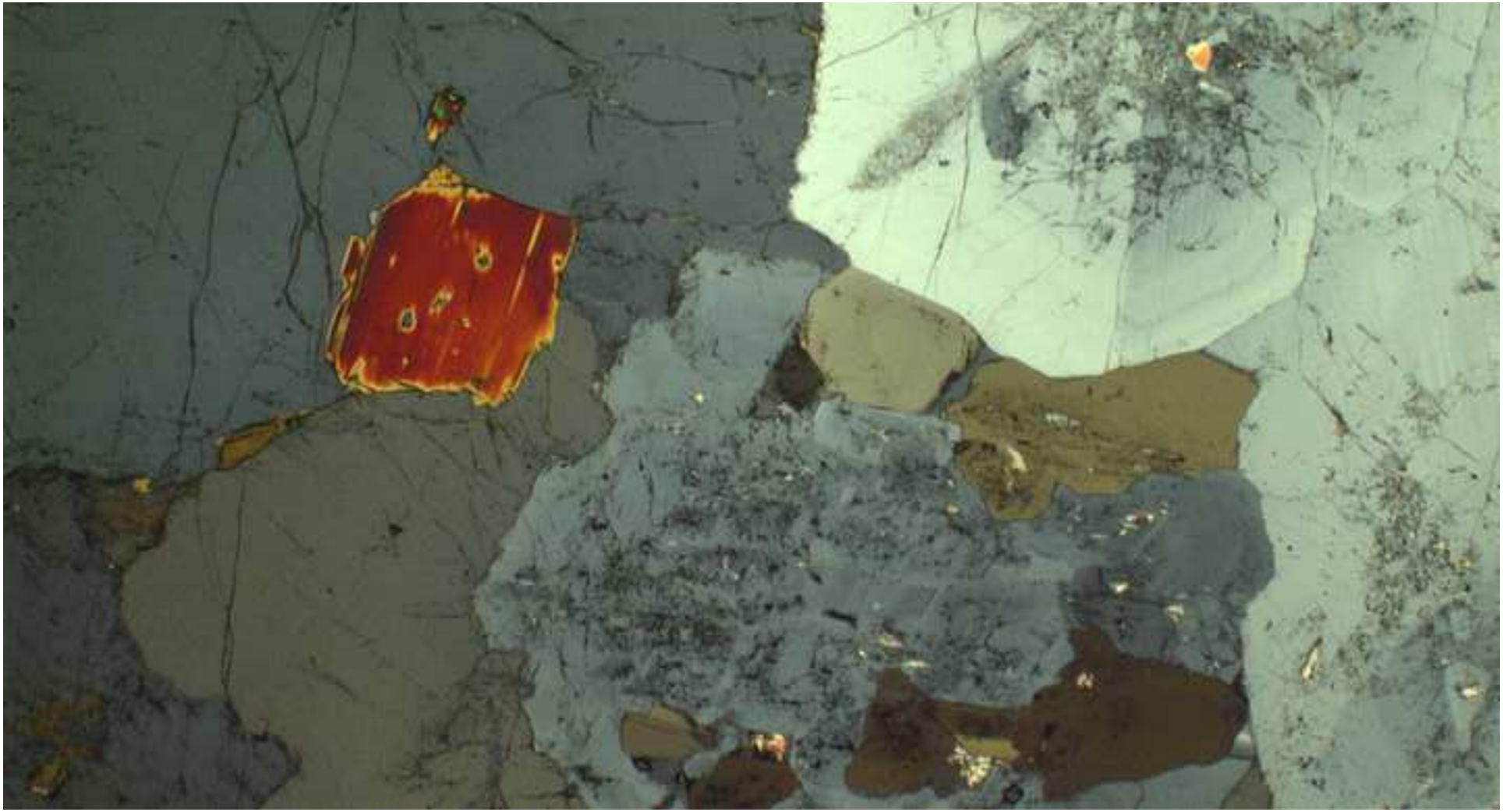

Figure4
Click here to download high resolution image

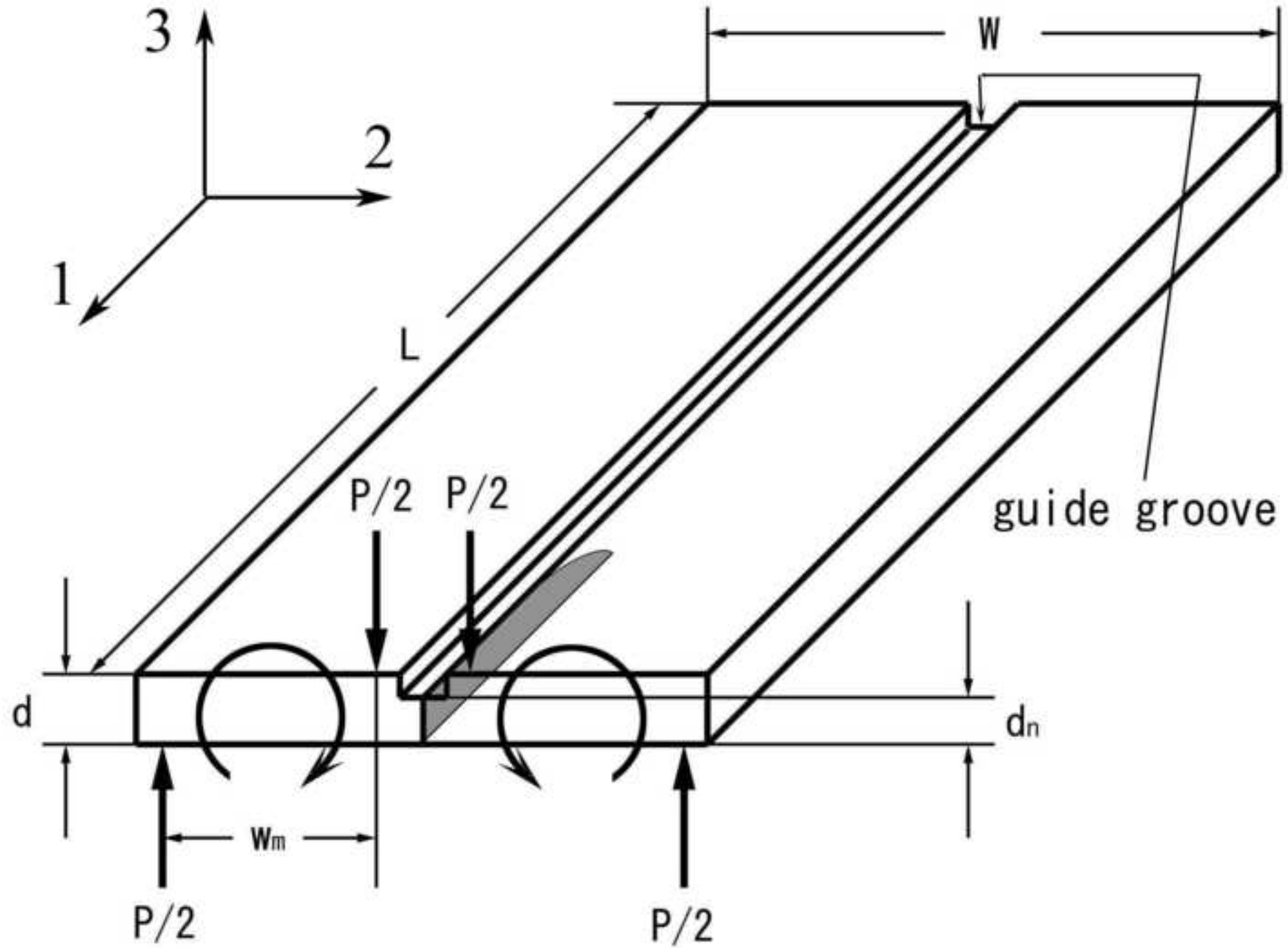

Figure5a
Click here to download high resolution image

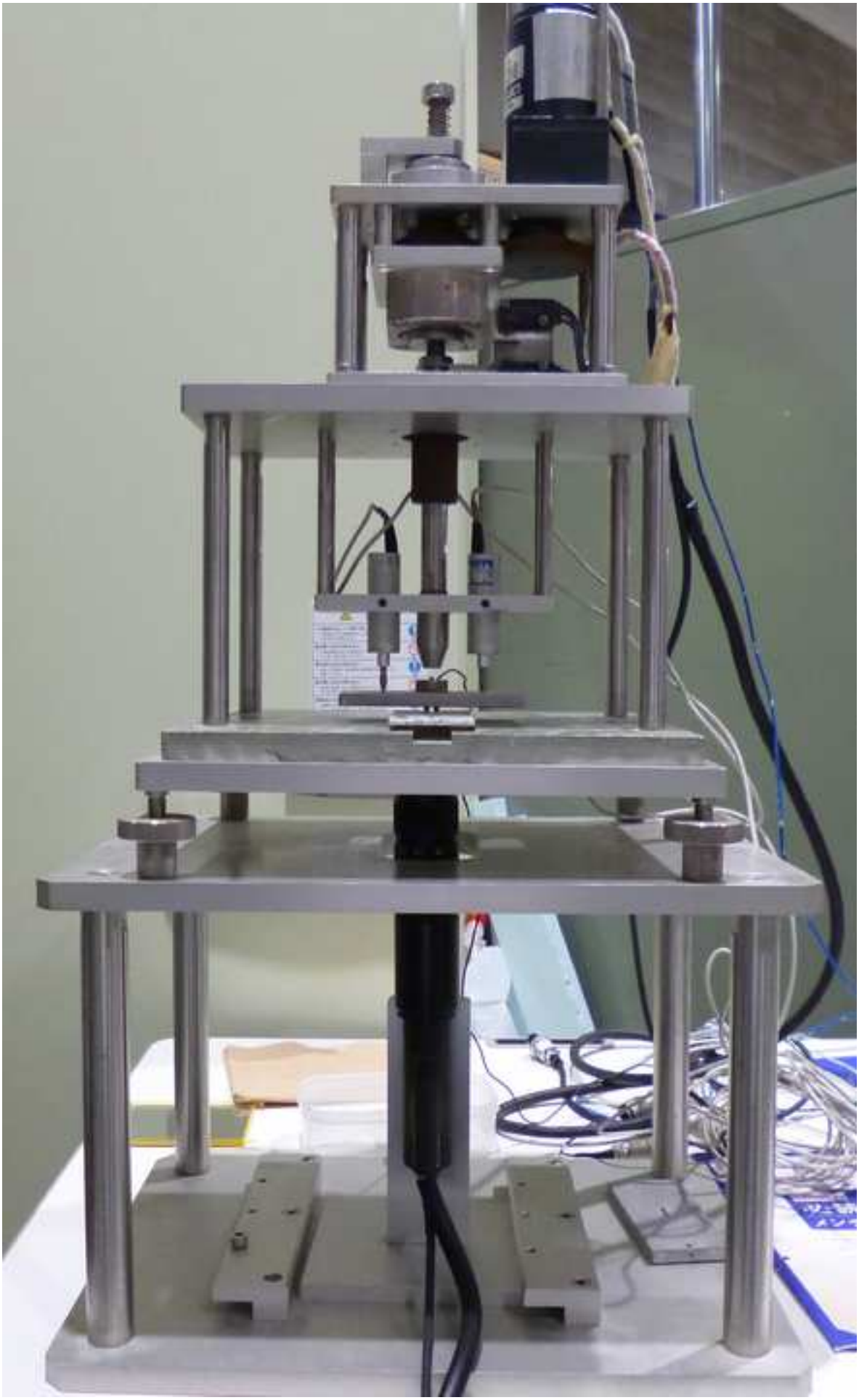

Figure5b
Click here to download high resolution image

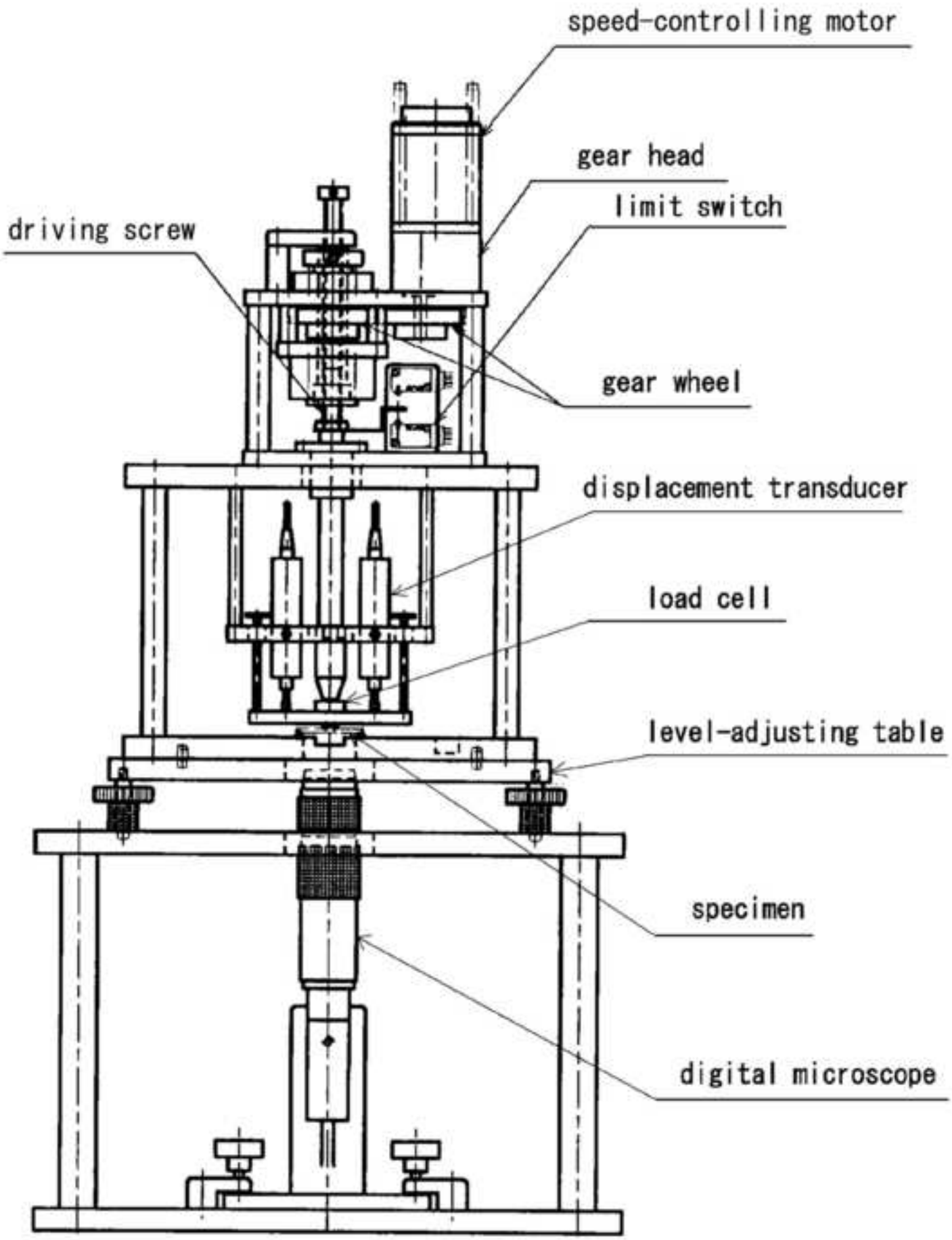

Figure6a
Click here to download high resolution image

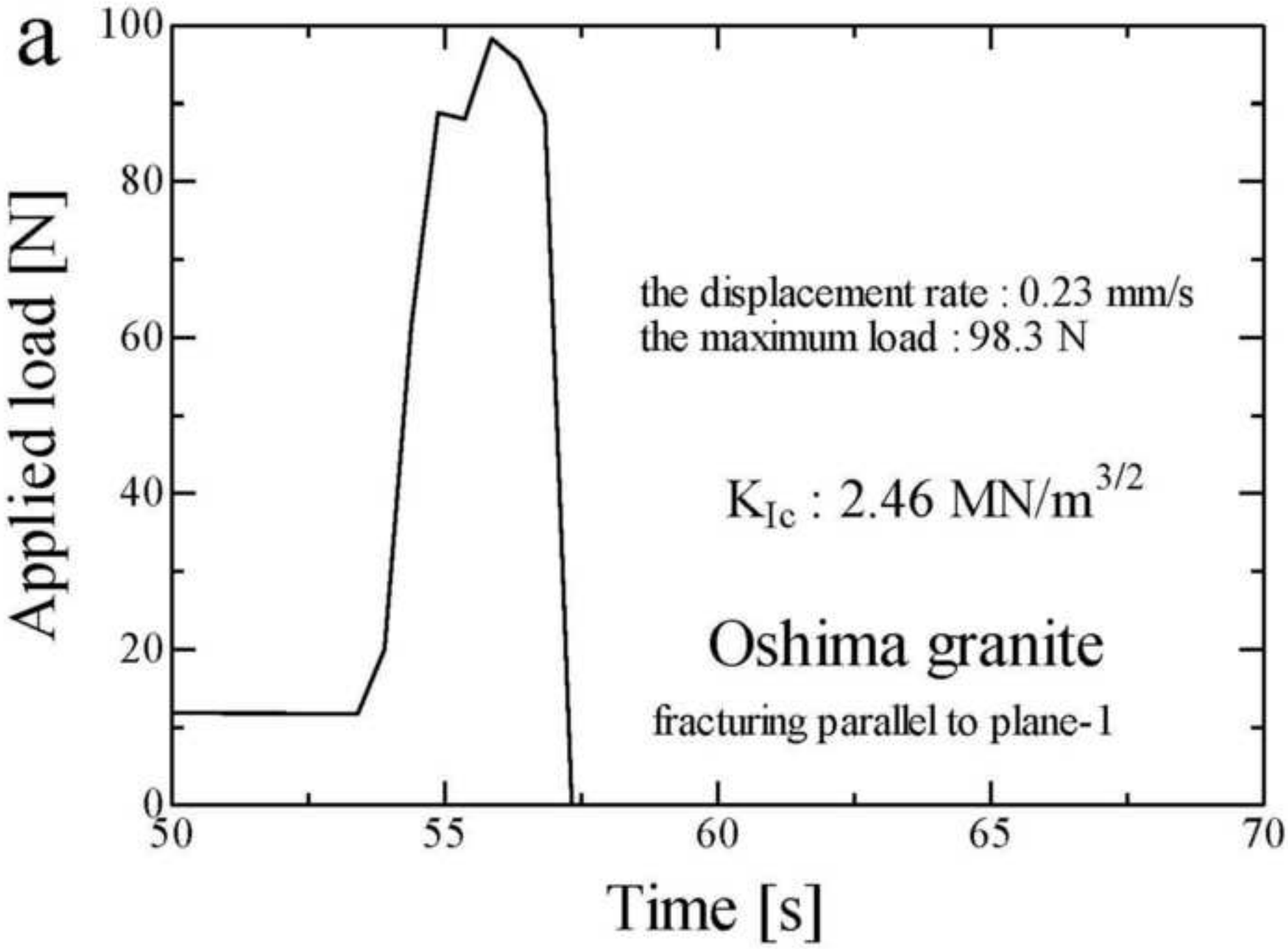

Figure6b
Click here to download high resolution image

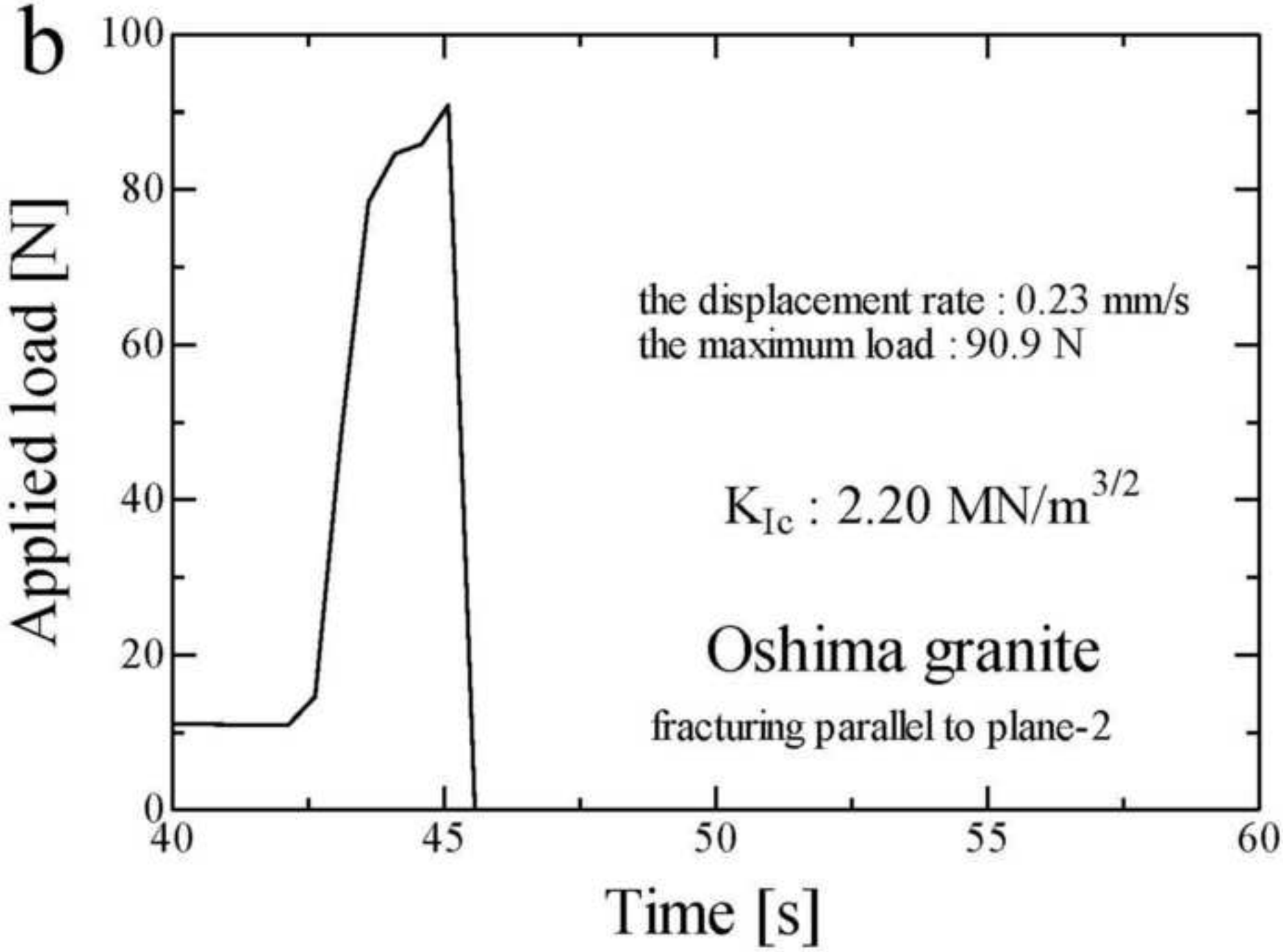

Figure6c
Click here to download high resolution image

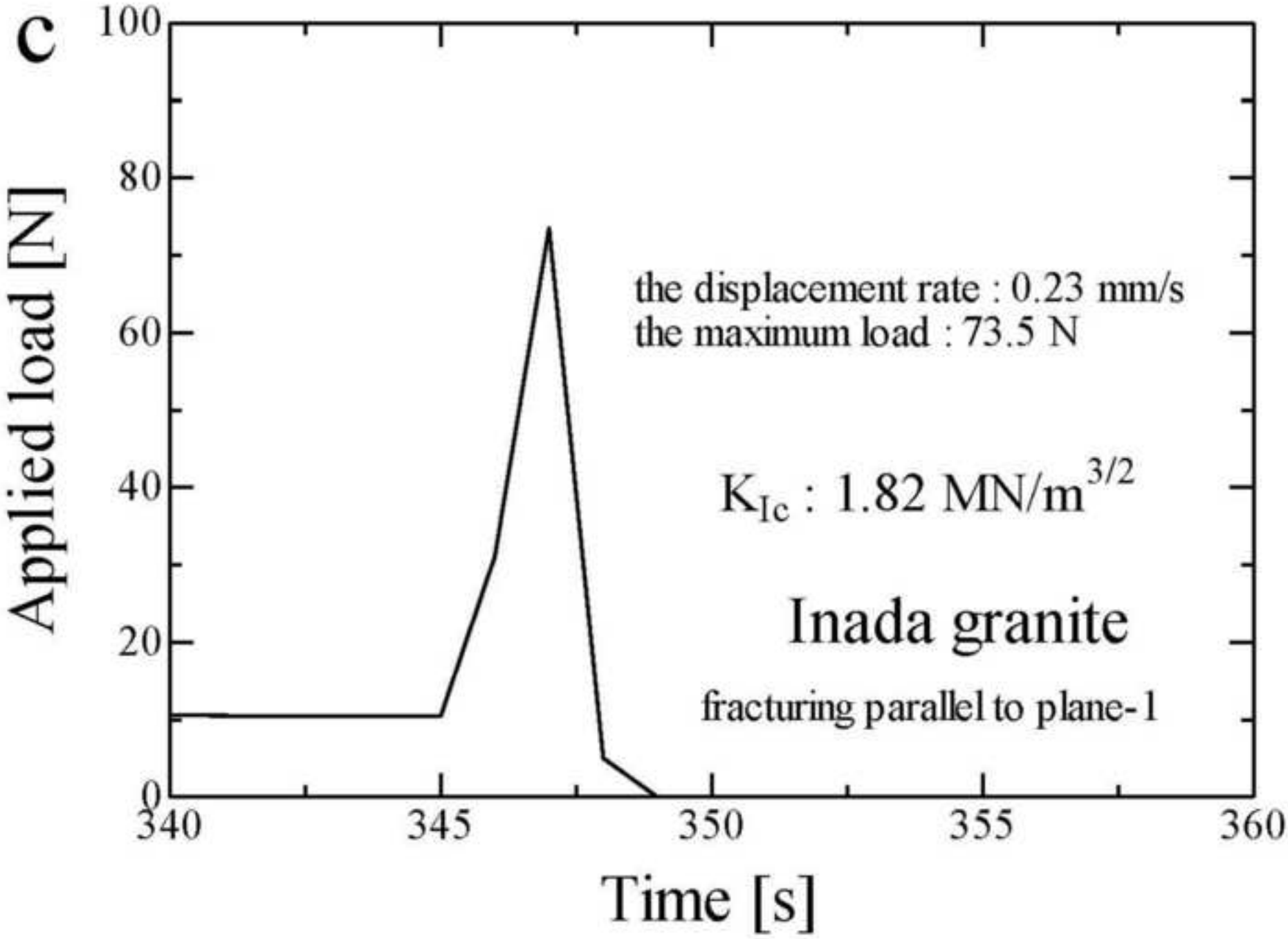

Figure6d
Click here to download high resolution image

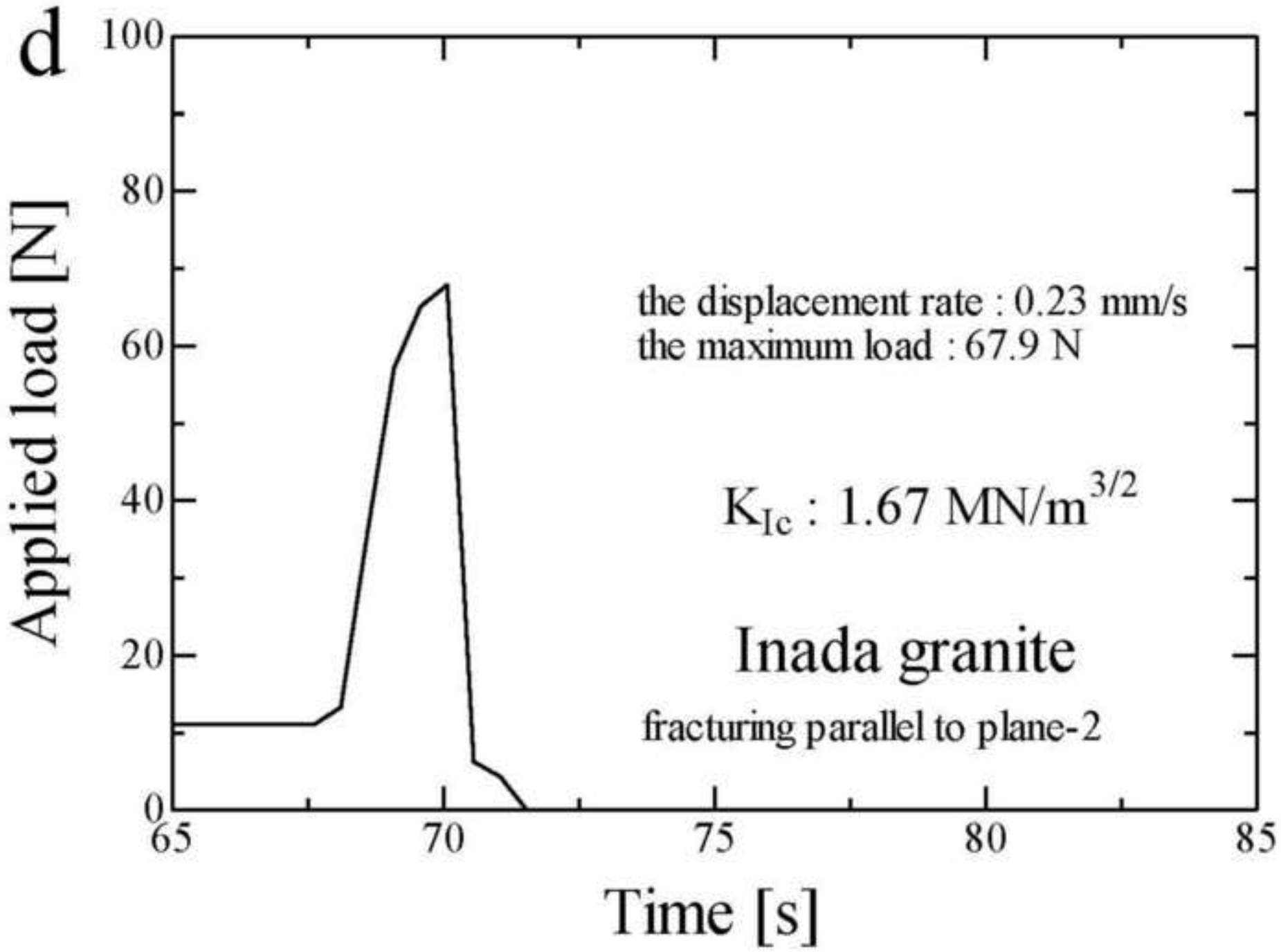

Figure6e
Click here to download high resolution image

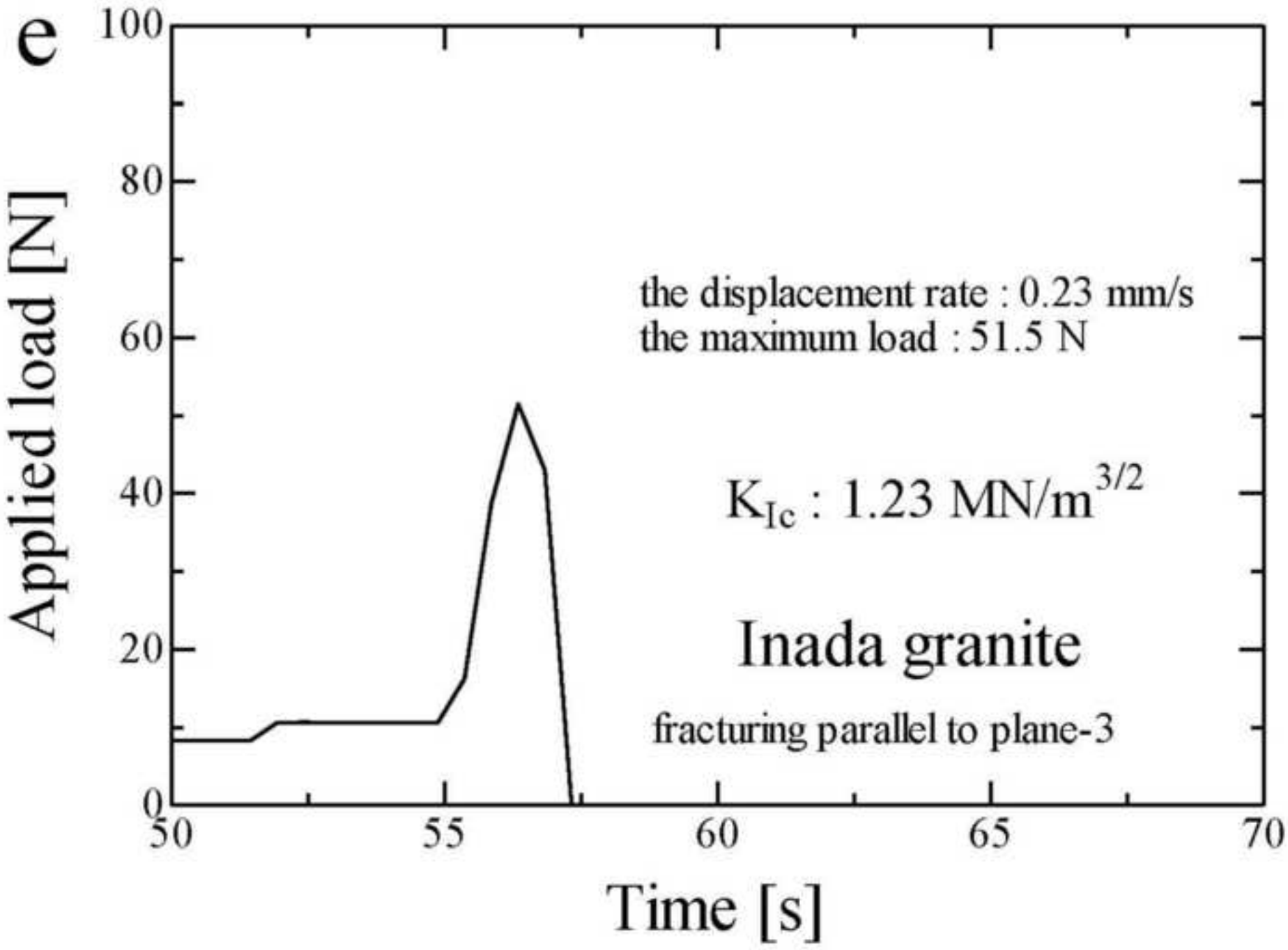

Figure7a
Click here to download high resolution image

Figure7b
Click here to download high resolution image

Figure8a
Click here to download high resolution image

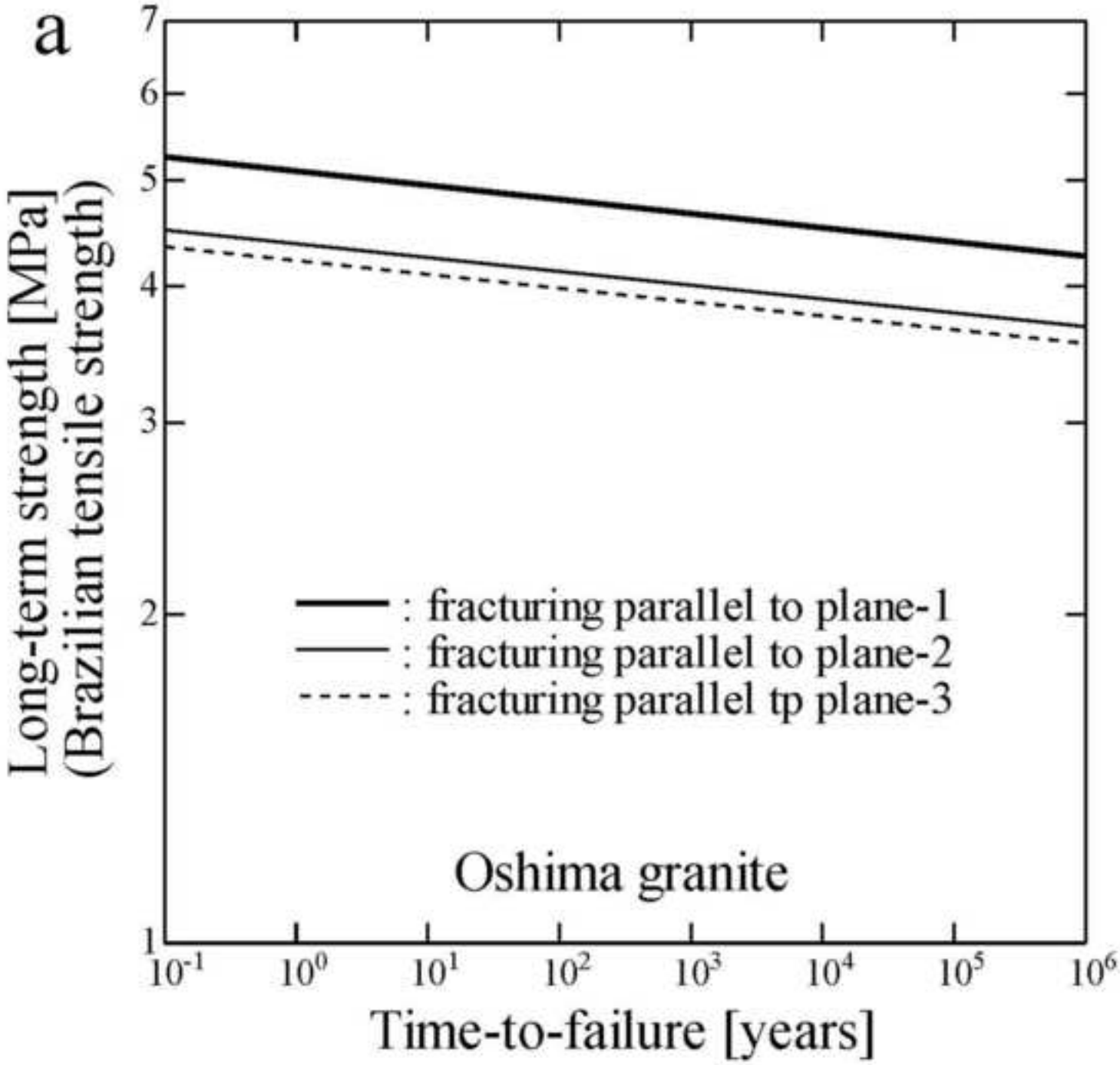

Figure8b
Click here to download high resolution image